Mantle convection, the asthenosphere, and Earth's thermal history

Scott D. King, Department of Geosciences, Virginia Tech, Blacksburg, VA 24061

Submitted: 15 August 2014
Revised: 24 January 2015
Accepted: 1 February 2015

Corresponding Author:
Scott King
Department of Geosciences
4044 Derring Hall
Virginia Tech
Blacksburg, VA 24060
Phone: 1-540-231-8954
e-mail: sdk@vt.edu

ABSTRACT

Calculations of mantle convection generally use constant rates of internal heating and time-invariant core-mantle boundary temperature. In contrast parameterized convection calculations, sometimes called thermal history calculations, allow these properties to vary with time but only provide a single average temperature for the entire mantle. Here I consider 3D spherical convection calculations that run for the age of the Earth with heat producing elements that decrease with time, a cooling core boundary condition, and a mobile lid. The calculations begin with a moderately hot initial temperature, consistent with a relatively short accretion time for the formation of the planet. I find that the choice of a mobile or stagnant lid has the most significant effect on the average temperature as a function of time in the models. However the choice of mobile versus stagnant lid has less of an effect on the distribution of hot and cold anomalies within the mantle, or planform. I find the same low-degree (one upwelling or two upwelling) temperature structures in the mobile lid calculations that have previously been found in stagnant-lid calculations. While having less of an effect on the mean mantle temperature, the viscosity of the asthenosphere has a profound effect on the pattern of temperature anomalies, even in the deep mantle. If the asthenosphere is weaker than the upper mantle by more than an order of magnitude, then the low-degree (one or two giant upwellings) pattern of temperature anomalies results. If the asthenosphere is less than an order of magnitude weaker than the upper mantle, then the pattern of temperature anomalies has narrow cylindrical upwellings and cold down going sheets. The low-degree pattern of temperature anomalies is more consistent with the plate model than the plume model (Foulger, 2007).

INTRODUCTION

Theories of convection in Earth's mantle extend as far back as Perry's argument refuting Kelvin's estimate of the age of the Earth (Perry, 1895; England et al., 2007). Holmes (1931, 1933) proposed that subsolidus convection, powered by heat from radioactive decay was the driving mechanism for plate tectonics, while Haskell (1935) showed that the uplift of Fennoscandia after the melting of the ice sheet could be modeled by viscous flow. Gilbert (1890) had previously described process similar to Haskell's model to explain the shorelines of ancient Lake Bonneville in western North America. Pekeris (1935) showed that thermal gradients near the surface could drive mantle convection. However, advancement of the theory of convection within the Earth's mantle accelerated during the plate tectonic revolution (c.f. Schubert et al., 2001; Bercovici, 2007).

The reader who is unfamiliar with the details of geodynamic modeling may not realize that there are two approaches to understanding mantle convection: one based only on an energy balance, which is sometimes called parameterized convection because a key relationship needed to create a single equation is a parameterization between heat flow and the Rayleigh number; and the second approach, which I will call Computational Fluid Dynamics (CFD), which solves the equations of conservation of mass, momentum, and energy on a gridded (usually) representation of the domain. Parameterized convection calculations are fast; one can perform 100's of calculations on a laptop in a day. CFD simulations in 3D spherical shell geometry require significant computer resources (e.g., a large cluster) and a single calculation can run from days to weeks. Parameterized convection provides a single average temperature for the entire mantle, while CFD solves for temperatures and velocities throughout the mantle.

Computational Fluid Dynamic Approach

The pioneering work on mantle convection was based on methodologies developed in the field of fluid mechanics applied to the Earth (Turcotte and Oxburgh, 1967; Schubert et al, 1969; Schubert and Turcotte, 1971; Richter, 1973; McKenzie et al., 1974; Richter and Johnson, 1974, Busse, 1975). For reasons of both intellectual and computational tractability, this early work focused on fluids with uniform material properties and small, two-dimensional, Cartesian domains. While these studies do not address many of the complexities associated with the Earth's interior, they produced enormous insight showing that: 1) mantle convection provides sufficient energy to drive plate motions (e.g., Turcotte and Oxburgh, 1967); 2) the phase transformation from ringwoodite to perovskite plus ferropericlase is not sufficient to act as a barrier to convection (e.g., Christensen and Yuen, 1984; 1985); 3) the long-wavelength geoid can be explained by subduction (e.g., Kaula, 1972; Chase, 1979; Anderson, 1982; Hager, 1984; Ricard et al. 1984); and 4) long-wavelength sea floor bathymetry can be explained by convection (Richter, 1973).

Modern numerical studies of mantle convection have addressed many of the unexplored complexities from the earlier studies including: non-linear temperature-dependent rheology (Torrence and Turcotte, 1971; Parmentier et al., 1976); compressibility (Jarvis and McKenzie, 1980; Leng and Zhong, 2008; King et al., 2010); three-dimensional geometry (c.f., Gable et al., 1991; Tackley et al., 1993; Lowman et al., 2001; 2003; 2004), self-consistent equations of state (Ita and King, 1994; 1998; Nakagawa et al., 2009); spherical geometry (Schubert and Zebib, 1980; Hager and O'Connell, 1981; Bercovici et al., 1989; Tackley et al., 1993; Bunge et al., 1997; Wen and Anderson, 1997a, 1997b; Zhong et al., 2000); the role of plates and slabs (Gurnis and Hager, 1988; Gurnis and Zhong, 1991; Zhong and Gurnis, 1992; King and Hager, 1994; Bercovici, 1995; Chen and King, 1998; Trompert and Hansen, 1998; Tackley, 2000; Billen and

Gurnis, 2003; Billen and Hirth, 2007; van Heck and Tackley, 2008, 2011; Billen, 2008, 2010; Coltice et al., 2013,2014).

Observation Plus Theory Approach

In parallel with the fluid dynamic approach, many researchers have followed an approach that makes direct use of observations, including: plate motions, seismic tomography models, geoid, dynamic topography, sea floor age, and heatflow, as direct constraints on fluid models. Anderson refers to this as the top-down approach (Anderson, 2001) because in most cases, the models first and foremost reproduce plate velocities. Pekeris (1935) might be the first to consider the geophysical top-down approach because he assumed that thermal gradients near the surface provided the perturbation that drives convection. Hager and O'Connell (1981) showed that slab geometry could be explained by viscous flow with imposed plate velocities. Forte and Peltier (1987) highlighted the important of toriodal (strike-slip) plate motions. In a uniform viscosity, or depth-dependent viscosity fluid buoyancy only produces poloidal, or rising and sinking, flow. Shear flow, or toroidal flow, requires a laterally-varying viscosity. We know that there is a significant component of toroidal, or shear, flow in the surface plate velocity field (i.e., major strike-slip faults such as the San Andreas). Many authors showed that the long-wavelength geoid could be explained by seismic anomalies in the lower mantle (Chase, 1979; Hager, 1984; Richard et al. 1984; Hager and Richards, 1989; Forte and Peltier, 1991; Forte et al., 1991; King and Masters, 1992). The approach of observation driven mantle models continues today (c.f., Becker and O'Connell, 2001; Becker and Boshi, 2002; Conrad and Lithgow-Bertelloni 2002, 2006; Conrad et al., 2007; Becker et al., 2009). Another important outcome of the above work is the necessity of a weak asthenosphere, a topic that I will return to later.

Parameterized Convection Approach

In contrast to the fluid mechanical approach to convection, the parameterized convection approach allowed researchers to balance heat lost through the surface of the Earth with heat from the formation of the Earth and radiogenic heat sources (Sharpe and Peltier, 1978, 1979; Schubert, 1979; Sleep, 1979; Davies, 1980; Turcotte, 1980). This approach made possible the study of the thermal evolution of the Earth using essentially analytic models. An extensive review of thermal history models can be found in Schubert et al. (2001). Here I give a simple overview.

For an incompressible fluid, the conservation of energy equation states that any change in temperature is related to the balance of the temperature advected into the region versus the heat that diffuses across the boundary and the heat generated internally. This is expressed by the equation below,

$$\rho c_v \left[\frac{\partial T}{\partial t} + \vec{u} \cdot \vec{\nabla} T \right] - \nabla q = \rho H, \qquad (1)$$

where ρ is the density of the fluid, c_v is the specific heat at constant volume, T is the temperature, t is time, $\vec{u}$ is the velocity of the fluid, q is the heat flux, and H is the rate of internal heat production per unit mass. The first term is the change in temperature with time. The second term is the temperature advection. The third term is the diffusion of heat and the final term is the internal heat generation. Integrating this equation over the volume of the mantle yields,

$$M c_v \frac{\partial \overline{T}}{\partial t} = MH - A\overline{q}, \qquad (2)$$

where M is the mass of the mantle and A is the area of the surface, $\overline{T}$ is the average temperature of the mantle, and $\overline{q}$ is the average surface heat flow. This assumes that there is no heat exchange between the mantle and the core, an assumption that can be later dropped by adding a similar equation for the thermal evolution of the core (c.f., Labrosse, 2003; Labrosse et al., 2007). The problem is that equation (2) has two unknowns, $\overline{T}$ and $\overline{q}$. What allows the parameterized convection formulation to take on a simple form is the substitution for the surface heat flux, making use of the relationship between heat flow and Rayleigh number (e.g., Chandrasekar, 1961; Solomatov, 1995):

$$Nu = \frac{q}{k(T - T_s)/d} = A\left(\frac{Ra}{Ra_{crit}}\right)^{\beta} \tag{3}$$

where Nu is the Nusselt number, the ration of heat flow to the heat flow due to conduction, T_s is the surface temperature, d is the depth of the mantle, k is the thermal conductivity, A and β are constants, and Ra is the Rayleigh number given by

$$Ra = \frac{\rho g \alpha \nabla T d^3}{\kappa \eta} \tag{4}$$

and Ra_{crit} is the critical value of the Rayleigh number for the onset of convection. In equation (4) g is the acceleration due to gravity, α is the coefficient of thermal expansion, κ is the thermal diffusivity, and η is the viscosity. It is straight-forward to add temperature-dependent viscosity and radiogenic heat sources that follow an exponential decay (Schubert et al., 1980; Davies, 1980; Schubert et al., 2001). In the case of temperature-dependent rheology, the value of viscosity used in the Rayleigh number has to be chosen and there are a variety of strategies. Some thermal history models have allowed for ρ, α, and κ to vary through the mantle (usually as a function of pressure). When these properties vary, the Rayleigh number is no longer sufficient to describe the problem without additional information. The relationship between heat flow and Rayleigh number, including the effect of temperature and stress dependent rheology, has been worked out in detail by Solomatov (1995). Furthermore, the analysis of Solomatov, which was based on a 2D Cartesian geometry, may need to be reevaluated for a 3D spherical geometry. Anderson (2004, 2005, 2013) raises the concern that calculations which ignore the pressure-dependence of the thermodynamic variables such as ϱ, α, and κ over-estimate the convective vigor in the lower mantle. When the density (ϱ) is allowed to vary, additional terms in the equation must be considered (c.f. Jarvis and McKenzie, 1980; Ita and King, 1994). The simplicity of the thermal history approach enables the calculation of thousands of models and systematic variation of parameters (Höink et al. 2013).

The value of the exponent β in equation (3) has been the source of considerable investigation. Boundary layer theory gives a value of 1/3 and many constant viscosity numerical investigations in 2D Cartesian geometry give values close to 0.3 (Schubert et al., 2001). When the viscosity is temperature-dependent, and the velocities near the surface tend toward zero, which is the stagnant lid mode of convection (Solomatov and Moresi, 1997) the value of β drops to nearly zero (Christensen, 1984) while with plate-like surface boundary conditions β is close to 0.3 (Gurnis, 1989). The value of β depends on the mechanics of the surface boundary layer, demonstrating that the surface plays mechanics plays an important role in the heat flow and hence thermal evolution of the Earth, consistent with arguments from Anderson (1994, 2001). It is important to point out that while this discussion has focused on the exponent β and the thermal history approach, the mechanics of the boundary layer has a critical role in CFD approaches to studying mantle convection as well.

Thermal history models have explored two effects that have been largely ignored by CFD studies of mantle convection: the decrease in radiogenic heat production and the decrease in core-mantle boundary temperature with time. CFD simulations of mantle convection have almost always used a constant core-mantle boundary temperature. The first use of a decreasing core-mantle boundary temperature in a mantle convection calculation was by Steinbach and Yuen (1994) who showed that the higher temperatures and resulting higher effective Rayleigh number early in Earth history leads to an endothermic phase transformation producing layered mantle convection early in Earth history, with a transition between layered and whole mantle convection occurring approximately 500 million to 1 billion years before present. No mantle convection simulations followed up on Steinbach and Yuen's results for Earth; however, Redmond and King (2004) suggested that due to a higher core temperature, Mercury's thin shell would have undergone subsolidus convection in the past and Sekhar and King (2014) showed that volcanism on Mars may have shut down due to the decrease in core-mantle boundary temperature.

As Anderson (2005,2013) has pointed out Earth accreted rapidly, perhaps in less than 5 Myrs, and thus the Earth began hot and has been cooling down ever since. There are some thermal history models where the mantle temperature increases soon after formation due to short-lived radionuclides; however this is a minor concern at this point. The high temperature starting condition for Earth's evolution, which has been extensively explored with thermal evolution models (c.f., Schubert et al., 2001), stands in contrast to CFD modeling of Earth's interior, which has often been carried out at steady state, statistical steady state, or only run for relatively short periods of time from carefully chosen initial conditions. The initial condition may control the final outcome of these models, especially because he argues that when properly accounting for pressure-dependence of thermodynamic properties in the lower mantle, the lower mantle should be modeled with a much lower Rayleigh number than most geodynamic calculations (Anderson, 2013). Anderson challenged the community to move away from the steady-state paradigm. The path to explore initial conditions is straight-forward and well understood. It simply requires additional calculations. As I will show below, there are some indicators in the calculations shown here that the effect of initial condition is not a significant concern, especially at high Rayleigh numbers. The climate community attempts to circumvent the uncertainty due to the initial conditions by ensemble averaging a large number of models. Such an approach has not yet been tried in mantle convection studies.

The work presented here will begin to assess the impact of decreasing radiogenic elements and core-mantle boundary temperature through time in 3D spherical convection simulations starting from a hot initial condition. The models build on two recent and important advances in mantle dynamics: the difference in mean temperature between Cartesian and spherical internally heated convection calculations (Shahnas et al., 2008; O'Farrell and Lowman, 2010; O'Farrell et al., 2013) and the impact of a weak asthenosphere on surface mobility of plates (Höink and Lenardic et al., 2008; Höink et al., 2011, 2012).

Radiogenic Elements and Mantle Convection

The heat produced by the decay of uranium, thorium and potassium is included in the convection equations through a rate of internal heating, play central roles in mantle dynamics and thermal evolution. The rates of internal heating that have been used in older Cartesian convection calculations always needed to be significantly smaller than geochemical estimates of abundances of radiogenic elements in the bulk silicate Earth (e.g., Šrámek et al. 2013). The approach often used in CFD studies has been to find a heating rate, by trial and error that generates some specified fraction of the total heat output, rather than using the geochemically determined abundances. Attempts to use actual abundances of radiogenic elements in Cartesian convection calculations have been shown to produce internal mantle temperatures that exceed the core-mantle boundary temperature (e.g., Redmond and King, 2004). We now recognize that reason for the heating imbalance in the older 2D Cartesian CFD studies had to do with the effect of spherical geometry. The surface area of a spherical-shell is larger than the surface area of a Cartesian domain when the same area of the base of the domain normalizes both domains. Consequently, a spherical-shell cools more rapidly than a Cartesian domain. Increasing the thickness of the spherical shell, decreases the mean temperature within the shell while holding all other parameters constant. Scaling relationships have been developed between spherical and Cartesian geometries enabling researchers to match internal temperatures in spherical and Cartesian geometry by rescaling the rate of internal heating (O'Farrell and Lowman, 2010; O'Farrell et al., 2013). Because the calculations here will use a spherical geometry, we do not need to worry about scaling.

There are large uncertainties in the abundances of heat producing elements. As pointed out by Šrámek et al. (2013), "estimates of the present-day heat-producing element (HPE) abundances in the bulk silicate Earth (BSE, defined as the entire Earth less its metallic core) vary by a factor of about three between different models (Turcotte and Schubert, 2002; O'Neill and Palme, 2008; Arevalo et al., 2009; Javoy et al., 2010)." This does not address how to partition the heat producing elements between the crust, upper mantle, and lower mantle. Anderson (2013) cautions that the current mismatch between geochemical abundances and heat budgets suggest that the physical assumptions underlying geochemical models are wrong.

The asthenosphere and convection

A low-viscosity relative to the lithosphere above and the upper mantle below characterize the asthenosphere. The viscosity of the asthenosphere has been estimated by glacial isostatic adjustment and geoid studies and estimates range from 10^{18} _10^{20} Pa s (c.f., Hager and Richards, 1989; King, 1995; Mitrovica 1996). Until recently, the role of the asthenosphere in mantle dynamics has been underappreciated (c.f., Anderson and King, 2014; Anderson and Natland, 2014). Many CFD studies have demonstrated that a low-viscosity asthenosphere can lead to long wavelength flow (e.g., Bunge et al., 1996, 1997; Tackley, 1996: Zhong and Zuber, 2001; Roberts and Zhong, 2006; Zhong et al., 2007). In addition, CFD studies have been able to generate a low-viscosity zone self consistently beneath a mobile lid through pressure- and temperature-dependent rheology (Tackley, 2000; Stein et al., 2004). The low-viscosity asthenosphere stabilizes horizontal large-scale flow by allowing material to move easily while minimizing the amount of viscous dissipation.

The importance of the asthenosphere in Earth's thermal evolution has been underscored by Höink and Lenardic (2008), "temperature in the mid and lower mantle decreases with increasing aspect ratio resulting in a sub-adiabatic lower mantle. This may require current thermal evolution models to be revised because it allows for an increased heat flux across the core-mantle boundary with increased convective wavelength. To date, thermal history studies that have considered the role of convective wavelength have assumed that longer wavelength cells are less efficient in cooling the mantle. Our results indicate that this will not be the case for mantle convection with an asthenosphere."

Rheology

Laboratory investigations recognize that the rheology of olivine is a function of temperature, pressure, stress, water content, and grain size (Hirth and Kohlstedt, 2003). Many geodynamicists take these microscopic creep laws and apply them at the macroscopic scale without considering the many orders of magnitude extrapolation between the laboratory conditions and the Earth. The effect of temperature and stress are largely considered to be the most significant effects on rheology, with approximately an order of magnitude decrease in viscosity for every 100°C increase in temperature or factor of 2 change in strain-rate (c.f., King, 2007). With the exception of slabs, the largest changes in temperature are radial, hence it is perhaps not surprising that depth-dependent viscosities are often a good approximation in geophysical models. It is especially sobering when you consider that there is a 100% uncertainty on the pressure dependence of the creep parameter, the activation volume (Hirth and Kohlstedt, 2003), and that geodynamic models often extrapolate the olivine rheology into the lower mantle (for lack of creep data on higher pressure phases), well beyond the olivine stability field. Geophysical observations have been generally reproduced by radial or layered viscosities, where the viscosity of each layer is uniform (c.f., King and Masters, 1992; Mitrovica, 1996) and convection calculations with uniform viscosity layers that are based on the average of a more complex temperature dependent rheology reproduce the major features of the more complex calculations (Christensen, 1984).

These observations do not negate the need to better understand mantle rheology, both from the laboratory and computational investigations, but they are intended to provide balance to the prevalent view that geophysical models must use the laboratory measured creep parameters in order to study the Earth. As pointed out in the previous section, Höink and Lenardic (2008) are able to produce a mobile lithosphere with uniform viscosity layers that vary only with depth. While these mobile lithosphere calculations do not have piecewise continuous velocities, as we expect for plates, previously Koglin et al. (2005) showed that the details of the plate generation method had little effect on the convective solution. Thus these mobile lithosphere calculations may be sufficient to understand many aspects of Earth's evolution.

METHOD

I use the spherical convection code CitcomS-3.2.0 (Zhong et al., 2000, 2008; Tan et al., 2006) with 64x64x64 or 96x96x96 elements in each of the 12 spherical caps. CitcomS solves the equations of conservation of mass, momentum and energy for a creeping, incompressible fluid (Schubert et al., 2001). The calculations use the Bousinessq approximation, which means that density, gravity, coefficient of thermal expansion, specific heat, and thermal diffusivity are all assumed to be constant. Anderson (2004, 2005, 2013) has pointed out that by ignoring these pressure effects the vigor of convection in the lower mantle is over-estimated. I compensate for this by using a lower Rayleigh number (equation 4) than is typically used in mantle convection studies (Table 1). For scaling purposes, I achieve the lower Rayleigh number by assuming that the scaling viscosity is 10^{22} Pa s rather than the more commonly assumed 10^{21} Pa s. I use a free-slip surface and core-mantle boundary and a depth-dependent viscosity following (Höink and Lenardic, 2008) to generate long-wavelength convection. The viscosity is independent of temperature and stress and is constant in for distinct layers, a lithosphere, asthenosphere, upper mantle and lower mantle (Figure 1). I consider two different rheologies, one with and one without an asthenosphere. For the non-asthenosphere case, the lithosphere is 90 km thick and has a viscosity that is 1000 times the reference viscosity, the upper mantle (90 to 670 km) uses the reference viscosity value, and the lower mantle (670 km to the core-mantle boundary) has a viscosity 30 times the reference viscosity (Figure 1). For the asthenosphere cases, the viscosity in the 90-400 km depth range is 0.01 times the reference viscosity. The choice of a depth-dependent viscosity is not only computationally expedient, it allows me to avoid the stagnant-lid mode of convection (Solomatov and Moresi, 1997), which would require not only temperature and pressure-dependent rheology but also a yield-stress, or damage formulation to mobilize the surface (Trompert and Hansen, 1998; Tackley, 2000; van Heck and Tackley, 2008). Koglin et al. (2005) has shown that the method of producing mobile plates has little impact on the dynamics of the system in 2D Cartesian domain. As I will show, the impact of a mobile surface in these calculations is significant; however, the effects due to the mechanism that I use to mobilize the surface are secondary for this problem.

I use radiogenic heat sources uniformly distributed throughout the entire mantle with abundances based on Turcotte and Schubert (2002) (Figure 2) and a core-mantle boundary temperature that decreases by 70 degrees per billion years based on Davies, 1980 (Figure 3). As discussed in the introduction, recent estimates of the abundances of heat producing elements in the bulk silicate Earth vary by a factor of three (Šrámek et al., 2013) and estimates of present core-mantle boundary temperature on Earth range from 3,300–4,300 K (Lay et al., 2008). The uncertainty in core-mantle boundary temperature will only increase going back through time. Both of these assumptions should be systematically explored; however a full exploration of this parameter space is beyond the scope of this work.

The initial temperature is 2173 $^{\circ}$C with 40 Myr half-space cooling solution and a 1% perturbation using a spherical harmonic degree and order 2,2; 4,2; 6,6; 20,10, and 40,20, pattern applied the interior. The harmonic perturbations are added and the resulting anomaly pattern is applied at five depths (270, 500, 1000, 1500 and 2000 km depth). This initial condition is used for all calculations in this paper. The parameters that determine the Rayleigh number and dimensional scaling for the models, which remain fixed in the calculations, are listed in Table 1.

RESULTS

I present a series of 3D spherical calculations to illustrate the effects of rheology, radiogenic heat sources (as opposed to a uniform rate of heating with time), and decreasing core-mantle boundary temperature with time on the average internal mantle temperature and planform of convection over the age of the Earth (Table 2).

Decaying Heat Sources and Decreasing Core-Mantle Boundary Temperature

The first calculation, DLA0, is a stagnant-lid convection calculation with a constant core-mantle boundary temperature of 2273^{o}C and constant rate of internal heating of 8×10^{-12} W kg^{-1}, which corresponds to present day heating using the values from Turcotte and Schubert (2002). This calculation has no asthenosphere, which means the viscosity as a function of depth follows the solid black line in Figure 1. The thermal structure at present day is illustrated by isotherms of temperature anomalies after removing the mean temperature at each radius. There are two scales of convection apparent in this model. There are eight uniformly-spaced upwellings that extend from the mantle to the surface and a smaller scale of upper mantle convective rolls illustrated by the sub-parallel linear features (Figure 4a). The rolls occupy regions between the upwellings in a near-equatorial and two polar bands. The upwelling geometry is consistent with a spherical harmonic degree 4 order 2 pattern, which is one of the perturbations in the initial condition. This pattern develops within the first 500 Myr of the calculation and remains stable throughout the rest of the calculation.

In order to illustrate cooling through time, I plot the radial variation of the temperature and Root-Mean Squared (RMS) velocity, where I use the v_θ and v_φ, components of velocity, integrated over the sphere at constant radius, r,

$$\overline{T}(r) = \int_0^{2\pi}\int_0^{\pi} T(r,\theta,\varphi) r^2 \sin(\theta) d\theta d\varphi \tag{5}$$

$$\overline{VH}(r) = \int_0^{2\pi}\int_0^{\pi} \sqrt{v_\theta(r,\theta,\varphi)^2 + v_\varphi(r,\theta,\varphi)^2}\, r^2 \sin(\theta) d\theta d\varphi. \tag{6}$$

In the plots which follow, I add a 0.3^oC/km adiabatic gradient to the $\overline{T}(r)$ as a function of radius plots, even though the model is Bousinessq, in order to facilitate comparison with adiabatic temperature profiles. Jarvis and McKenzie (1980) show that to first-order, the results of compressible flow are equal to incompressible flow plus an adiabatic gradient. $\overline{T}(r)$ and $\overline{VH}(r)$ as a function of radius are plotted every 500 Myr of model evolution in Figure 5a and b respectively. The peak in $\overline{VH}(r)$ that occurs in the middle of the upper mantle because the uniform viscosity of the upper mantle (10^{22} Pa s) is smaller than the lithosphere above (10^{25} Pa s) and the lower mantle below (3×10^{23} Pa s) and the flow is fastest in the region of lowest viscosity. $\overline{T}(r)$ and $\overline{VH}(r)$ are nearly constant with time, showing that the calculation has settled into a quasi-steady state within the first 500 Myr of model evolution. Near the surface $\overline{VH}(r)$ is close to zero, showing that the calculation is in the stagnant-lid convection regime (Solomotov and Moresi, 1997). The temperature below the lithosphere exceeds 2000 $^{\circ}$C in calculation DLA0, illustrating that the stagnant lid does not efficiently remove heat from the mantle.

When I repeat the calculation allowing for internal heat generation based on radioactive decay (Figure 2) and including decreasing core-mantle-boundary temperature (Figure 3), I find that the deep upwelling structures seen in calculation DLA0 are absent and the calculation is dominated by the short wavelength rolls in the upper mantle with broad, isolated anomalies in the lower mantle (Figure 4b). The plots of $\overline{T}(r)$ and $\overline{VH}(r)$ as a function of radius (Figure 6a and b) are similar to those from calculation DLA0 although in the case of DLA1, $\overline{T}(r)$ decreases with time. This is to be expected as both the internal heat sources and core-mantle boundary temperature decrease with time. As was the case with calculation DLA0, the near the surface value of $\overline{VH}(r)$ is close to zero; however $\overline{T}(r)$ as a function of radius is even larger in calculation DLA1 than was the case in calculation DLA0. This is because for most of the calculation, the heat production term is larger in DLA1 than DLA0, as the heat production term in DLA0 is based on present day heat production and the amount of Heat Producing Elements (HPEs) increases with time in the past.

In order to compare these calculations with thermal evolution models, I integrate the temperature (including the adiabatic gradient) over the volume of the mantle with time and present the mean temperature as a function of time in Figure 7. In contrast to calculation DLA0, which is almost unchanged from it’s initial state over 4.5 Gyr of model, calculation DLA1 heats up for the two billion years, and then cools by almost 400 degrees over the last two and a half billion years of the calculation. Consistent with the plots of $\overline{T}(r)$ as a function of radius, the average mantle temperatures (Figure 7) are unrealistically large. For example, in both DLA0 and DLA1, the temperature immediately below the top thermal boundary layer is 2000 $^{\circ}$C, which is significantly hotter than any reasonable estimate of mantle temperature at 100-200 km depth (e.g., Anderson, 2013).

While these calculations vary two properties at one time, which is generally not the best practice for understanding complex systems, it is necessary to generate a calculation with mantle temperatures that are more in line with the Earth before investigating the effect of internal heating and core-mantle boundary temperature individually. Thus the next series of calculations will focus on producing present day geotherms that are more consistent with the Earth.

Adding an asthenosphere

The next calculation, DLA2, is otherwise identical to calculation DLA1 except that I include an asthenosphere in the radial viscosity following the dashed-dot line in Figure 1. The change in planform is dramatic, with a ring of upwelling material and downwelling material 90 degrees apart (Figure 4c). The upwelling material extends from the core (red sphere) to the surface, while the blue surface only extends part way through the mantle. This planform is typical of stagnant-lid convection with a viscosity increase with depth (Zhong and Zuber, 2001; Roberts and Zhong, 2006; Zhong et al., 2007). The plot of $\overline{VH}(r)$ as a function of radius has a larger peak in velocity at a shallower depth compared with DLA0 and DLA1, reflecting the lower viscosity (10^{20} Pa s) in the asthenosphere (Figure 8b) and the plot of $\overline{T}(r)$ as a function of radius decreases with time (Figure 8a) more rapidly than in DLA1 (Figure 6a) indicating that the weak asthenosphere aids in removing heat from the system by allowing more material to circulate through the asthenosphere than in the model without it. Comparing the mean mantle temperature from calculation DLA2 (red line in Figure 7) with the previous calculations, the increase in temperature early in the calculation is not as large as was the case for calculation DLA1 and the mantle cools more rapidly. While there is a major planform difference between DLA1 (Figure 4b) and DLA2 (Figure 4c), it is the difference in the flow velocity in the asthenosphere that leads to the difference in the mean mantle temperature (Figure 7).

The Affect of Lithosphere Mobility

To assess the impact of the stagnant lid on the thermal evolution I reduce the lithosphere viscosity to 100 (DLA3) and 10 (DLA4) times the reference viscosity with all other properties identical to calculation DLA2. Both the thermal evolution (green line in Figure 7) and planform of calculation DLA3 (not shown) are nearly identical to calculation DLA2. In the near surface, $\overline{VH}(r)$ is approximately 10 mm/yr, significantly greater than zero but still small relative to the deeper flow. Calculation DLA4 has a convection pattern with a single broad upwelling in one hemisphere and a broad downwelling in the other hemisphere (Figure 4d), sometimes called a degree-1 pattern because of its correspondence with the degree-1 spherical harmonic. Once again, this temperature pattern has been previously recognized in stagnant-lid convection with a viscosity increase with depth (Zhong and Zuber, 2001; Roberts and Zhong, 2006; Zhong et al., 2007). Here I show that the same pattern develops even with a mobile lid. In DLA4, in value of $\overline{VH}(r)$ near the surface is larger than the value of $\overline{VH}(r)$ in the lower mantle, although smaller than $\overline{VH}(r)$ in the upper mantle (Figure 9a). In calculation DLA4 the thermal boundary layer is approximately 100 km thick and the mantle temperature directly beneath the lithosphere is approximately 1500 $^{\circ}$C (Figure 9b), both of which are closer to Earth values than those in the previous calculations. The impact of the mobile lithosphere is to flux warm material across the surface where it can cool efficiently. Then the cool, near-surface material sinks back into the mantle. The surface velocities from calculation DLA4 are plotted on the temperature isosurface plot (Figure 4d) in order to make the point that while the lithosphere in this calculation is mobile, the near-surface velocities are not piecewise continuous. There is significant strain across the surface and these calculations do not reproduce plate-like behavior. However it is notable just how significant the mobile surface is at cooling the mantle.

The Affect of Rate of Internal Heat Generation

In an effort to explore the tradeoff between rheology and rate of internal heating, I considered calculations otherwise identical to calculation DLA4 except for a constant (with time) rate of internal heating equal to the present day value (DLA5), a constant (with time) rate of internal heating equal to the average value over the 4.5 Gyr of Earth history (DLA6) (Table 2). DLA5 and DLA6 have patterns of temperature anomalies and plots of $\overline{VH}(r)$ and $\overline{T}(r)$ as a function of radius that are similar to DLA4 (Figures 4d and 9 respectively). The mean mantle temperature as a function of time (Figure 7) for these calculations follows a sensible progression. Comparing the smallest constant rate of internal heating the mobile surface simulation (DLA5 - yellow curve on Figure 7) cools off much faster than the stagnant lid simulation (DLA0 - black curve on Figure 7). Here in DLA0 the CMB temperature is constant while in DLA5 it is decreasing, but as I will show in the next section, the decreasing CMB temperature plays a secondary role to lithospheric mobility. For the larger but constant rate of internal heating with a mobile surface (DLA6 - yellow curve on Figure 7), the mantle cools slower than DLA5 (mobile surface smaller rate of heating), but still significantly faster than DLA0 (smaller heating, stagnant lid). Hence whether or not the simulation has a mobile lithosphere has a larger effect on mean mantle temperature than the range of internal heating parameters considered.

The Affect of Core Mantle Boundary Temperature

The affect of CMB temperature is illustrated by considering the difference between DLA6 and DLA7, both of which have mobile lids, and a constant (with time) rate of internal heating equal to the average value over the 4.5 Gyr of Earth history (Table 2). Once again, DLA6 and DLA7 have patterns of temperature anomalies and plots of $\overline{VH}(r)$ and $\overline{T}(r)$ as a function of radius that are similar to DLA4 (Figures 4d and 9 respectively). The difference being that the CMB temperature of DLA7 remains fixed while DLA6 decreases but the difference is only seen in the thermal boundary layer at the CMB. The impact of the CMB temperature on the mean mantle temperature can be seen by comparing the yellow (DLA6) and black (DLA7) curves on Figure 7. The two curves overlap for the first billion years of model evolution. This makes sense because the only difference is the temperature at the core mantle boundary, which changes by only about 3% (70 degrees out of 2200) in the first billion years. Then between one and two billion years, the mean mantle temperature for the constant core mantle boundary temperature calculation is lower than the decreasing core mantle boundary temperature calculation, reflecting a difference in the evolution of the flows. After two billion years, the mean mantle temperature of the decreasing CMB temperature case (yellow curve) is lower than the mean mantle temperature of the constant CMB temperature case (black curve). This is to be expected because the lower temperature at the core mantle boundary provides less heat to the mantle. The fact that the decreasing core mantle boundary temperature has a small effect on the mantle temperature is not surprising because in these calculations, like the Earth, most of the heat is generated by radioactive decay, rather than heating from the core below (e.g., Davies, 1980).

Higher Rayleigh Number and Systematic Variation of Asthenosphere Viscosity

To address the question of whether the low Rayleigh number in these calculations is the cause of the long-wavelength structure, I consider three additional calculations with a Rayleigh number 10 times that of the previous set of calculations. These simulations have a scaling viscosity of 10^{21} Pa s and are in the range of resent day estimates of mantle Rayleigh number. Because of the higher Rayleigh number, these calculations are computed on a 96x96x96 element cubed-sphere grid. The mean mantle temperature as a function of time curves for these calculations are shown in Figure 10, along with the mean mantle temperature for calculation DLA4 (mobile lithosphere, radiogenic heat sources, decreasing core temperature boundary condition) for comparison. Calculation DLA9 (blue curve) is identical to calculation DLA4 (black curve) except for the order of magnitude increase in Rayleigh number, achieved by decreasing the scaling viscosity. The planform of the calculation single upwelling in one hemisphere and a downwelling in the other hemisphere (Figure 11b), very similar to the lower Rayleigh number calculation DLA4 (Figure 11a). It is important to note that there is no degree-1 structure in the initial conditions, so I have confidence that the pattern of hot and cold temperature anomalies is not being controlled by the initial condition. With greater convective vigor, it is not surprising that this calculation has a shorter initial warming period and begins cooling earlier in time as seen in the mean mantle temperature curve (Figure 10). Calculation DLA10 (red curve on Figure 10) is identical to calculation DLA9 except that the asthenosphere viscosity is increased from 0.01 times the background to 0.03 times the background. The pattern of hot and cold temperature anomalies in calculation DLA10 (Figure 11c) is dominated by a single giant upwelling in one hemisphere much like DLA4 (Figure 11a) and DLA9 (Figure 11b). There is more structure in this upwelling, which looks more like a cluster of plumes as opposed to the single massive upwelling seen in

Figure 11a. However, the temperature structure is dominated by one anomalously hot hemisphere and one anomalously cold hemisphere. When the asthenosphere viscosity is increased to 0.3 times the reference viscosity (DLA11) the pattern of hot and cold temperature anomalies is completely different (Figure 11d). In this case the pattern of hot and cold temperature anomalies is narrow upwellings and downwelling sheet planform, first described by Bercovici et al. (1989). Interestingly, the mean mantle temperature for this case closely follows that of the lower Rayleigh number and low viscosity asthenosphere simulation (DLA4), which has the one anomalously hot hemisphere and one anomalously cold hemisphere planform (Figure 10). Hence the mean mantle temperature, which is the primary output of thermal history calculations, is not a good predictor of the convective planform. Even with a fairly simple model, where I hold almost all parameters fixed and vary the Rayleigh number, lithosphere and asthenosphere viscosities, and rate of internal heating, I find multiple patterns of mantle convection that produce nearly the same mean mantle temperature.

DISCUSSION

The reader familiar with thermal history calculations will no doubt immediately recognize that the calculations here begin at a low initial mantle temperature and I have chosen a larger mantle viscosity than typically used in mantle convection studies. I chose to begin from a lower initial temperature because I do not have sufficient numerical resolution for the high-Rayleigh number conditions of the early Earth. These are best seen as numerical experiments designed to understand the interaction between physical parameters as opposed to simulations of the Earth. As such, trying to directly compare these calculations with the Earth or previous thermal history calculations would be unproductive.

These calculations only begin to explore the parameter space for the thermal history of the Earth, yet there are some interesting observations that can be drawn. First, the role of the mobile lithosphere is critical. This is certainly not a novel observation, as many others have made it before (e.g., Bunge et al., 1996, 1997; Tackley, 1996: Zhong and Zuber, 2001; Roberts and Zhong, 2006; Zhong et al., 2007). It is quite interesting that in these calculations I have included no yield-stress, damage theory, or plate breaking criterion; I simply have a very weak asthenosphere and somewhat weak lithosphere. This produces not only long-wavelength flow but also a mobile lithosphere as has been previously shown by Höink and Lenardic (2008) and others. This mobile lithosphere does not produce piecewise rigid caps and the degree to which that might impact the mean mantle temperatures in these calculations is at present unknown. Including a yield-stress rheology with thermal history calculations is an ongoing project. Whether the lithosphere was mobile or rigid had by far the largest impact on the thermal evolution of the calculations. In this regard, I confirm the result of Höink and Lenardic (2008) that long-wavelength flow cools the mantle more efficiently than previous work has shown. The question of when plate tectonics as we know it began on Earth is critical to understanding Earth's thermal history (see Stern's article in this volume). A simple exercise will illustrate the point. Models of the formation of the Earth suggest that accretion happened rapidly and that after the moon-forming giant impact the Earth was molten. It would have cooled rapidly due to the mobile surface. As the Earth continued to cool, its thermal history would be significantly altered by whether or not it went into a stagnant lid phase of convection before plate tectonics began. If the Earth entered a stagnant lid phase of convection, cooling would be significantly reduced and cooling would have slowed or perhaps even stopped. When the Earth finally entered the plate tectonic phase, rapid cooling would have resumed. The results here show that even if an early phase of plate tectonics were different than what we observe today, a mobile lid phase of convection would allow for rapid cooling.

While the onset of plate tectonics is important for many aspects of Earth's evolution, based on this work perhaps an equally important question is whether there has always been a weak asthenosphere. In *New Theory of the Earth*, Anderson lays out three first-order questions of mantle dynamics: 1) Why does Earth have plate tectonics?; 2) What controls the onset of plate tectonics, the number, shape and size of the plates, and the onset or plate reorganization?; 3) What is the organizing principle for plate tectonics is it driven or organized from the top or by the mantle? What if anything is *minimized*? Indeed, the onset time of plate tectonics is critical based on this work while the number, shape and size of plates may or may not impact the results presented here.

A second observation based on these calculations is that the long-wavelength pattern of convection and the single large upwelling (i.e., degree-1 convection) persists even in calculations where there is strong internal heating and (relatively) high mantle temperatures, as would be expected in the early Earth (e.g., DLA4). This is not really a surprising result because it is well-known that convection predominantly heated from within has broad, diffuse upwellings (e.g., McKenzie et al., 1974). Zhang et al. (2010) have suggested that Earth's mantle may oscillate between degreee-1 convection during supercontinent assemblage and degree-2 convection and that the Large Low Shear Velocity Provinces (LLSVPs) at the base of the mantle beneath African and the south Pacific which are observed in seismic topographic images may be a reflection of this long-wavelength, degree-2 convection pattern. This leads to the obvious question, where are the narrow upwelling plumes and can they exist within this long-wavelength mode of convection? It is striking that these calculations do not resemble many narrow upwelling plumes pattern of convection that is envisioned by many deep Earth geoscientists. The models here are much more consistent with the plate model of Foulger (2007) than the plume model.

Next, unless the decrease in core-mantle boundary temperature is dramatically larger than what I considered here (e.g., 300 degrees over the age of the Earth), the effect of core-mantle boundary temperature will be minimal. Indeed, this does not seem very controversial because estimates put the contribution of core heat to the total heat flow at the surface at about 10% (e.g., Davies, 1988; King and Adam, 2014). This is certainly a question that deserves more attention; however because I have explored a very limited number of calculations here and these calculations lack consistent heat exchange between the core and mantle further discussion does not seem justified.

Finally, perhaps the most interesting and no doubt controversial suggestion is that the planform of the deep mantle may be controlled by the strength of the asthenosphere. With a weak asthenosphere, the simulations produce very long-wavelength structures (one or two hot anomalies). This planform is consistent with the two observed LLSVPs that have been a consistent feature of mantle tomographic models. The cylindrical upwelling, downwelling sheet planform requires an asthenosphere viscosity that is no more than a factor of 10 weaker than the upper mantle. There is ample geophysical evidence (c.f., Hager, 1984; King, 1995; Mitrovica, 1996) that the asthenosphere is weaker than this. In fact, because asthenosphere means ‘weak layer’, the concept of a strong asthenosphere is an oxymoron.

At this point the reader will note that I have gone to lengths to avoid using the term ‘plume’ to describe the cylindrical upwellings in these calculations. My reason for doing so is the confusion that has come by various different researchers and research areas using the term to mean something different. For example, the LLSVPs near the base of the mantle have been called superplumes by some authors (e.g., Romonowicz and Gung, 2006) but in many ways these structures more appropriately described as Large Low Shear Velocity Provinces (LLSVP) because calling them superplumes or thermochemical piles already gives a specific interpretation to the observation. The cylindrical upwellings in DLA0 are certainly 'plumes' in the way that researchers in fluid mechanics would use that term but are certainly broader and have a larger thermal anomaly than 'mantle plumes' in the sense proposed by Morgan (1971). As Anderson, Lustrino, and Eugenio point out on the mantleplume.org website, the list of types of plumes described in the literature include: fossil, dying, recycled, tabular, finger-like, baby, channeled, toroidal, head-free, cold, depleted residual, pulsating, throbbing, subduction-fluid fluxed, refractory, zoned, cavity, diapiric, starting, impact, incubating, incipient, splash, passive, primary, secondary, satellite, strong, weak, tilted, parasite, thermo-chemical, asymmetric, fluid dynamic, depleted, stealth, lateral, CMB, shallow, 670-, mega-, super-, mini-, cacto, cold-head, headless, petit, implausible (IMP), and plumelet.

CONCLUSIONS

I have considered eleven 3D spherical convection simulations that start from a hot mantle and cool for the age of the Earth, examining the planform of convection and the mean mantle temperature as a function of time. The simulations vary the rate of internal heating, core temperature boundary condition, viscosities of the lithosphere and asthenosphere, and Rayleigh number. The effect of a variable core-mantle-boundary temperature is minimal. The most significant effects were the lithosphere and asthenosphere viscosity.

A strong lithosphere (stagnant lid) leads to higher mean mantle temperatures while a mobile lid leads to lower mean mantle temperatures. Low-degree convection patterns have been previously reported in stagnant-lid calculations (e.g., Zhong and Zuber, 2001), I find identical low-degree patterns in mobile lid calculations with a weak asthenosphere. A significant caveat at this point is that while the lithosphere in these calculations is mobile, it is not piecewise constant or plate-like. It is unknown what impact plate-like surface velocities will have on this result.

The viscosity of the asthenosphere controls the pattern of convection in the mantle (even the deep mantle). Calculations with a weak asthenosphere (more than 10 times weaker than the upper mantle) have long-wavelength flow patterns with one or two massive upwellings. Calculations with a stronger asthenosphere (less than 10 times weaker than the upper mantle) have many cylindrical upwellings and downwelling sheets, a planform that goes back to Bercovici et al. (1989). Given our present understanding of the asthenosphere, this work suggests that the long-wavelength anomalies seen in seismic tomography models more closely reflects the structure of the lower mantle than a series of narrow, upwelling plumes.

Acknowledgements

S. D. King acknowledges funding from the *Alexander von Humboldt Foundation* and Advanced Research Computing at Virginia Tech for providing computational resources and technical support URL: http://www.arc.vt.edu I also acknowledge constructive and encouraging comments from Don Anderson, who read an early draft of this manuscript and reminded me that while computing is fun, there can be great value in going back and reading the classics. Figures were made with Generic Mapping Tools (Wessel and Smith, 1998).

References

Anderson, D. L., 1967, Phase changes in the upper mantle: Science, v. 157, p. 1165–1173, 1967.
Anderson, D. L., 1982, Hotspots, polar wander, Mesozoic convection, and the geoid: Nature, v. 297, p. 391–393.
Anderson, D. L., 1994, Superplumes or supercontinents?: Geology, v. 22, p. 39–42.
Anderson, D. L., 1995, Lithosphere, asthenosphere and perisphere: Reviews of Geophysics, v. 33, p. 125–149.
Anderson, D. L., 1998, The scales of mantle convection: Tectonophysics, v. 284, p. 1–17.
Anderson, D. L., 2000, The thermal state of the upper mantle; no role for mantle plumes: Geophysical Research Letters, v. 27, p. 3623–3626.
Anderson, D. L. 2000, The statistics and distribution of helium in the mantle: International Geology Review, v.42, p. 289–311.
Anderson, D. L., 2001, Top-down tectonics: Science, v. 293, p. 2016–2018.
Anderson, D. L., 2002, How many plates?: Geology, v. 30, p. 411–414.
Anderson, D.L., 2004, Simple scaling relations in geodynamics; the role of pressure in mantle convection: Chinese Science Bulletin, v. 49, p. 2017–2021.
Anderson, D.L. 2005, Self-gravity, self-consistency, and self-organization in geodynamics and geochemistry, in Earth's Deep Mantle: Structure, Composition, and Evolution, Eds. R.D. van der Hilst, J. Bass, J. Matas and J. Trampert, AGU Geophysical Monograph Serie, v. 160, p. 165–186.
Anderson, D. L., 2007, New Theory of the Earth. Cambridge University Press, Cambridge, UK.
Anderson, D. L., 2013, The persistent mantle plume myth. Australian Journal of Earth Science, v. 60, p. 657–673.
Anderson, D. L., and King, S. D., 2014, Driving the Earth machine? Science, v. 346, p. 1176–1177.
Anderson, D. L., and Natland, J. H., 2014, Mantle updrafts and mechanisms of oceanic volcanism Proceedings of the National Academy of Science, v. 111, E4298.
Anderson, D. L., Tanimoto, T., and Zhang, Y., 1992, Plate tectonics and hotspots: the third dimension: Science, v. 256, p. 1645–1651.
Arevalo Jr., R., McDonough, W.F., and Long, M., 2009, The K/U ratio of the silicate Earth: insights into mantle composition, structure and thermal evolution. Earth and Planetary Science Letters, v. 278, p. 361–369, doi:10.1016/j.epsl. 2008.12.023.
Becker, T. W. and O'Connell, R. J., 2001, Predicting plate velocities with mantle circulation models, Geochemistry, Geophysics and Geosystems, v.2, 1060, doi:10.1029/2001GC000171.
Becker, T. W. and Boschi, L., 2002, A comparison of tomographic and geodynamic mantle models: Geochemistry, Geophysics and Geosystems, v. 3, 1003, doi:10.1029/2001GC000168.
Becker, T.W., Conrad, C.P., Buffett, B., and Müller D.R., 2009, Past and present seafloor age distributions and the temporal evolution of plate tectonic heat transport: Earth and Planetary Science Letters, v. 278, p. 233–242, doi:10.1016/j.epsl.2008.12.007.
Bercovici, D., 1995, A source-sink model of the generation of plate tectonics from non-Newtonian mantle flow: Journal of Geophysical. Research, v. 100, p. 2013-2030.
Bercovici, D., 2003, The generation of plate tectonics from mantle convection: Earth and Planetary Science Letters, v. 205, p. 107-121.

Bercovici, D., 2007, Mantle dynamics, Past, Present and Future: An Overview, in Treatise on Geophysics, vol. 7, Mantle Dynamics, D. Bercovici editor; G. Schubert, editor in chief, Elsevier, New York; Ch. 1 pp. 1-30.

Bercovici, D., Schubert, G. and Glatzmaier, G. A., 1989, Three-dimensional, spherical models of convection in the Earth's mantle: Science, v. 244, p. 950–955.

Billen, M. I., 2008, Modeling the dynamics of subducting slabs: Annual Reviews of Earth and Planetary Science, v. 36, p. 325-356, doi:10.1146/annurev.earth36.031207.124129.

Billen, M. I., 2010, Slab dynamics in the transition zone: Physics of the Earth and Planetary Interiors, v. 183, p. 296-308, doi:10.1016/j.pepi.2010.05.005

Billen, M. I. and Gurnis, M. 2003, A comparison of dynamic models in the Aleutian and Tonga-Kermadec subduction zones: Geochemistry, Geophysics and Geosystems, v. 4, 1035, doi:10.1029/2001GC000295.

Billen, M. I., and Hirth, G. 2007, Rheologic controls on slab dynamics: Geochemistry, Geophysics and Geosystems, v. 8, Q08012, doi:10.1029/2007GC001597.

Bunge, H.-P., Richards, M.A., and Baumgardner, J.R., 1996, Effect of depth-dependent viscosity on the planform of mantle convection: Nature, v. 379, p. 436–438, doi: 10.1038/379436a0.

Bunge, H.-P., Richards, M.A., and Baumgardner, J.R., 1997, A sensitivity study of three-dimensional spherical mantle convection at 108 Rayleigh number: Effects of depth-dependent viscosity, heating mode, and an endothermic phase change: Journal of Geophysical Research, v. 102, p. 11,991–12,008.

Busse, F.H., 1975, Patterns of convection in spherical shells: Journal of Fluid Mechanics, v. 72, p. 67–85, doi: 10.1017/S0022112075002947.

Chandrasekhar, S., 1961, Hydrodynamic and Hydromagnetic Stability. Oxford, pp. 654.

Chase, C. G., 1979, Subduction, the geoid, and lower mantle convection: Nature, v. 282, p. 464–468.

Chen, J., and King, S. D., 1998, The influence of temperature and depth dependent viscosity on geoid and topography profiles from models of mantle convection: Physics of the Earth and Planetary Interiors, v. 106, p. 75–91.

Christensen, U. R., 1984, Heat transport by variable viscosity convection and implications for the Earth's thermal evolution: Physics of the Earth and Planetary Interiors, v. 35, p. 264–282.

Christensen U. R., 1996, The influence of trench migration on slab penetration into the lower mantle: Earth and Planetary Science Letters, v. 140, p. 27–39.

Christensen, U. R., 2001, Geodynamic models of deep subduction: Physics of the Earth and Planetary Interiors, v. 127 p. 25–34.

Christensen, U. R., and Yuen, D. A., 1984, The interaction of a subducting lithospheric slab with a chemical or phase boundary: Journal of Geophysical Research, v. 89, p. 4389–4402.

Christensen, U. R., and Yuen, D. A., 1985, Layered convection induced by phase transitions: Journal of Geophysical Research, v. 90, p. 291–300.

Coltice, N., T. Rolf and P. J. Tackley, Seafloor spreading evolution in response to continental growth (2014), Geology, doi:10.1130/G35062.1.

Coltice, N., Seton, M., Rolf, T., Müller, R. D., and Tackley, P. J., 2013, Convergence of tectonic reconstructions and mantle convection models for significant fluctuations in seafloor spreading. Earth and Planetary Science Letters, v. 383, p. 92–100.

Conrad, C. P., and Lithgow-Bertelloni C., 2002, How mantle slabs drive plate tectonics: Science, v. 298, 207–209, doi:10.1126/science.1074161

Conrad, C. P., and Lithgow-Bertelloni, C., 2006, Influence of continental roots and asthenosphere on plate-mantle coupling, Geophysical Research Letters, v. 33, L05312, doi:10.1029/2005GL025621.

Conrad, C. P., Behn, M. D., and Silver, P. G., 2007, Global mantle flow and the development of seismic anisotropy: Differences between the oceanic and continental upper mantle Journal of Geophysical Research, v. 112, B07317, doi:10.1029/2006JB004608.

Davies, G. F., 1980, Thermal histories of convective Earth models and constraints on radiogenic heat production in the Earth: Journal of Geophysical Research, v. 85, p. 2517–2530.

England, P., Molnar, P., and Richter, F., 2007, John Perry's neglected critique of Kelvin's age for the Earth: A missed opportunity in geodynamics: GSA Today, v. 17, no. 1, p. 4–9.

Foulger, G.R., 2007, The "Plate" model for the genesis of melting anomalies, in Plates, Plumes, and Planetary Processes, G.R. Foulger and D.M. Jurdy (Eds.), Geological Society of America Special Paper v. 430, 1–28.

Forte, A. M., and Peltier, W. R., 1987, Plate tectonics and aspherical Earth structure: The importance of poloidal-toroidal coupling: Journal of Geophysical Research, v. 92, p. 3645–3679.

Forte, A. M., and Peltier, W. R., 1991, Viscous flow models of global geophysical observables; 1, Forward problems: Journal of Geophysical Research, v. 96, p. 20,131–20,159

Forte, A. M., W. R. Peltier, and A. M. Dziewonski, 1991, Inferences of mantle viscosity from tectonic plate velocities, Geophysical Research Letters, v. 18, p. 1747–1750.

Frost, D. J., 2008, The upper mantle and transition zone: Elements, v. 4, p. 171–176.

Gable, C. W., O'Connell, R. J . and Travis, B. J., 1991, Convection in three dimensions with surface plates: Generation of toroidal flow: Journal of Geophysical Research, v. 96, p. 8391–8405.

Gilbert, G. K., 1890, Lake Bonneville. USGS Monograph, v. 1, 438 pp.

Gurnis, M., 1989, A reassessment of the heat transport by variable viscosity convection with plates and lids: Geophysical Research Letters, v. 16, p. 179–182.

Gurnis M, and Hager, B. H., 1988, Controls on the structure of subducted slabs: Nature, v. 335, p. 317–22.

Gurnis, M. and Zhong, S., 1991, Generation of long-wavelength wavelength heterogeneity in the mantle by the dynamic interaction between plates and convection: Geophysical Research Letters, v. 18, p. 581–584.

Hager, B.H., 1984, Subducted slabs and the geoid: Constraints on mantle rheology and flow: Journal of Geophysical Research, v. 89, p. 6003–6016.

Hager, B. H. and O'Connell, R. J., 1981, A simple global model of plate dynamics and mantle convection: ,Journal of Geophysical Research, v. 86, p. 4843–4867.

Hager, B. H., and Richards, M. A., 1989, Long-wavelength variations in Earth's geoid: Physical models and dynamical implications, Philosophical Transactions of the Royal Society of London, Series A, v. 328, p. 309–327.

Haskell, N.A., 1935, The motion of a viscous fluid under a surface load, I. Physics, v. 6, p. 265–269.

Hirth, G., and Kohlstedt, D., 2003, Rheology of the upper mantle and the mantle wedge: A view from the experimentalists, in Inside the Subduction Factory, Geophysical Monograph Series, v. 138, edited by J. Eiler, p. 83–105 AGU, Washington, D. C.

Höink, T., and Lenardic, A., 2008, Three-dimensional mantle convection simulations with a low-viscosity asthenosphere and the relationship between heat flow and the horizontal length scale of convection: Geophysical Research Letters, v. 35, L10304. doi:10.1029/2008GL033854

Höink, T., Jellinek, A. M., and Lenardic, A., 2011, Asthenosphere drive: A wavelength-dependent plate-driving force from viscous coupling at the lithosphere-asthenosphere boundary. Geochemistry, Geophysics and Geosystems, v. 12, Q0AK02, doi:10.1029/2011GC003698, 2011.

Höink, T., Lenardic, A. and Richards, M. A., 2012, Depth-dependent viscosity and mantle stress amplification: implications for the role of the asthenosphere in maintaining plate tectonic: Geophysical Journal International, v. 191, p. 30–41, doi:10.1111/j.1365-24X2012.o5621.x,

Höink, T, Lenardic, A. and Jellinek, A.M., 2013, Earth's thermal evolution with multiple convection modes: A Monte-Carlo Approach: Physics of the Earth and Planetary Interiors, v. 221, p. 22–26.

Holmes, A., 1931, Radioactivity and earth movements, Geological Society of Glasgow Transactions, v. 18, p. 559–606.

Holmes, A., 1933, The thermal history of the earth: Journal of the Washington Academy of Science, v. 23, p. 169–195.

Ita, J.,J., and King, S. D., 1994, The sensitivity of convection with an endothermic phase change to the form of governing equations, initial conditions, aspect ratio, and equation of state: Journal of Geophysical Research, v. 99, p. 15,919–15,938.

Ita, J.,J., and King, S. D., 1998, The influence of thermodynamic formulation on simulations of subduction zone geometry and history: Geophysical Research Letters, v. 25, 1463–1466, doi: 10.1029/98GL51033.

Jarvis, G.T. and McKenzie, D.P., 1980, Convection in a compressible fluid with infinite Prandtl number: Journal of Fluid Mechanics, v. 96, p. 515–583.

Javoy, M., et al., 2010, The chemical composition of the Earth: enstatite chondrite models: Earth and Planetary Science Letters, v. 293, p. 259–268, doi:10.1016/ j.epsl.2010.02.033.

Kaula, W. M., 1972, Global gravity and tectonics. In E. C. Robinson (ed.) The Nature of the Solid Earth, New York, McGraw-Hill, p. 386–405.

King, S.D., 1995, The viscosity structure of the mantle. In: Reviews of Geophysics (Supplement) U.S. Quadrennial Report to the IUGG 1991-1994, p. 11–17.

King, S.D., 2007, Mantle downwellings and the fate of subducting slabs: Constraints from seismology, geoid, topography, geochemistry, and petrology. in *Treatise on Geophysics, Volume 7, Mantle Dynamics*, pp. 325–370.

King, S. D., and Adams, C., 2014, Hotspot swells revisited: Physics of the Earth and Planetary Interiors, v. 235, p. 66–83.

King, S.D., and Hager, B. H., 1994, Subducted slabs and the geoid: 1) Numerical calculations with temperature-dependent viscosity. Journal of Geophysical Research, v. 99, p. 19,843–19,852.

King, S. D., and Ita, J. J., 1995, The effect of slab rheology on mass transport across a phase transition boundary. Journal of Geophysical Research, v. 100, p. 20,211–20,222.

King, S.D., and Masters, G., 1992, An inversion for radial viscosity structure using seismic tomography. Geophysical Research Letters, v. 19, p. 1551-1554.

King, S.D., Lee, C., van Keken, P.E., Leng, W., Zhong, S., Tan, E., Tosi, N., and Kameyama, M. C., 2010, A community benchmark for 2-D Cartesian compressible convection in the Earth's mantle: Geophysical Journal International, v. 180, p. 73–87, doi: 10.1111/j.1365-246X.2009.04413.x.

Koglin Jr., D. E., Ghias, S., King, S. D., Jarvis, G. T., and Lowman, J. P., 2005, Mantle convection with mobile plates: A benchmark study: Geochemistry, Geophysics and Geosystems, v. 6, Q09003, doi:10.1029/2005GC000924.

Lay, T., Hernlund, J., and Buffett, B. A., 2008, Core-mantle boundary heat flow: Nature Geosciences, v. 1, p. 25–32, doi:10.1038/ngeo.2007.44
Lee, C., and King, S.D., 2011, Dynamic buckling of subducting slabs reconciles geological observations: Earth and Planetary Science Letters, v. 312, p. 360–370, doi:10.1016/j.epsl.2011.10.033
Leng, W. and Zhong, S., 2008, Viscous heating, adiabatic heating and energetic consistency in compressible mantle convection: Geophysical Journal International, v.173, p. 693–702.
Lowman, J.P., King, S.D., and Gable, C.W., 2001, The influence of tectonic plates on mantle convection patterns, temperature and heat flow: Geophysical Journal International, v. 146, p. 619–637.
Lowman, J.P., King, S.D., and Gable, C.W., 2003, The role of the heating mode of the mantle in periodic reorganizations of the plate velocity field: Geophysical Journal International, v.152, p. 455–467.
Lowman, J.P., King, S.D., and Gable, C.W., 2004, Steady plumes in viscously stratified, vigorously convecting, 3D numerical mantle convection models with mobile plates, Geochemistry Geophysics Geosystems, v. 5, 10.1029/2003GC000583.
McKenzie, D.P., Roberts, J.M., and Weiss, N.O., 1974, Convection in the earth's mantle: Towards a numerical simulation: Journal of Fluid Mechanics, v. 62, p. 465–538, doi: 10.1017/S0022112074000784.
Meibom, A., and Anderson, D. L., 2004, The statistical upper mantle assemblage: Earth and Planetary Science Letters, v. 217, p, 123–139.
Mitrovica, J. X., 1996, Haskell (1935) revisited: Journal of Geophysical Research, v. 101, p. 555–569.
Morgan, W. J., 1971, Convection plumes in the lower mantle: Nature, v. 230, p. 42-43.
Nakagawa, T., Tackley, P. J., Deschamps, F., and Connolly, J. A. D., 2009, Incorporating self-consistently calculate mineral physics into thermo-chemical mantle convection simulations in a 3D spherical shell and its influence on seismic anomalies in Earth's mantle: Geochemistry, Geophysics and Geosystems, v.10, Q03004, doi:10.1029/2008GC002280.
O'Farrell, K.A., and Lowman, J.P., 2010, Emulating the thermal structure of spherical shell convection in plane-layer geometry mantle convection models: Physics of the Earth and Planetary Interiors, v. 182, p. 73–84, doi:10.1016/j.pepi.2010.06.010.
O'Farrell, K.A., Lowman, J. P. and Bunge, H.-P., 2013, Comparison of spherical-shell and plane-layer mantle convection thermal structure in viscously stratified models with mixed-mode heating: implications for the incorporation of temperature-dependent parameters: Geophysical Journal International, v. 192, p. 456–472.
O'Neill, H.S., Palme, H., 2008, Collisional erosion and the non-chondritic composition of the terrestrial planets: Philosophical Transactions of the Royal Society of London A, v. 366, p, 4205–4238, doi:10.1098/rsta.2008.0111.
Parmentier, E. M., Turcotte, D. L.. and Torrance, K. E., 1976, Studies of finite amplitude non-Newtonian thermal convection with application to convection in the Earth's mantle: Journal of Geophysical Research, v. 81, 18–39.
Pekeris, C. L., 1935, Thermal convection in the interior of the Earth. Geophysical Journal International, v. 3., p. 343–367.
Perry, J., 1895, On the age of the earth: Nature, v. 51, p. 224–227.
Redmond, H. L., and King, S. D., 2007, Parameterized thermal history calculations vs. full convection models: Applications to the thermal evolution of Mercury: Physics of the Earth and Planetary Interiors, v. 164, p. 221–231.

Ricard, Y., Fleitout, L., and Froidevaux, C., 1984, Geoid heights and lithospheric stresses for a dynamic earth: Ann. Geophys. v. 2, p. 267–286.
Richards, M.A., and Hager, B. H., 1984. Geoid anomalies in a dynamic Earth: Journal of Geophysical Research, v. 89, p. 5987–6002.
Richter, F. M., 1973, Dynamical models of sea floor spreading: Reviews of Geophysics and Space Physics: v. 11, p. 223–287.
Richter, F.M., and Johnson, C.E., 1974, Stability of a chemically layered mantle: Journal of Geophysical Research, v. 79, p. 1635–1639.
Richter, F.M., Nataf, H. C., and Daly, S. F., 1983, Heat transfer and horizontally averaged temperature of convection with large viscosity variations: Journal of Fluid Mechanics, v. 129 p. 173–192.
Roberts, J. H., and Zhong, S., 2006, Degree-1 convection in the Martian mantle and the origin of the hemispheric dichotomy: Journal of Geophysical Research, v. 111, E06013, doi:10.1029/2005JE002668.
Romanowicz, B. and Gung, Y., 2006, Superplumes from the core-mantle boundary to the lithosphere: implications for heat flux: Science, v. 296, p. 513-516.
Schubert, G., 1979, Subsolidus convection in the mantles of terrestrial planets: Annual Review of Earth and Planetary Sciences, v. 7, p. 289–342, doi: 10.1146/annurev.ea.07.050179.001445.
Schubert, G., and Turcotte, D.L., 1971, Phase changes and mantle convection: Journal of Geophysical Research, v. 76, p. 1424–1432.
Schubert, G. and Zebib, A., 1980, Thermal convection of an internally heated infinite Prandtl number fluid in a spherical shell: Geophysical and Astrophysical Fluid Dynamics, v. 15, p. 65–90.
Schubert, G., Turcotte, D.L. and Oxburgh, E. R.. 1969, Stability of planetary interiors: Geophysical Journal of the Royal Astronomical Society, v. 18, p. 705–735.
Schubert, G., Turcotte, D.L., and Olson, P., 2001. Mantle Convection in the Earth and Planets. Cambridge Univ. Press, New York. 940 pp.
Sekhar, P., and King, S. D., 2014, 3D spherical models of Martian mantle convection constrained by melting history: Earth and Planetary Science Letters, v. 388, p. 27–37.
Shahnas, M.H., Lowman, J.P., Jarvis, G.T., and Bunge, H-.P., 2008, Convection in a spherical shell heated by an isothermal core and internal sources: implications for the thermal state of planetary mantles: Physics of the Earth and Planetary Interiors, v. 168, p. 6–15, doi:10.1016/j.pepi.2008.04.007, 2008
Sharpe, H.N. and Peltier, W.R., 1978, Parameterized mantle convection and the earth's thermal history: Geophysical Research Letters, v. 5, p. 737–740, doi:10.1029/GL005i009p00737.
Sharpe, H. N. and Peltier, W. R., 1979, A thermal history model for the Earth with parameterized convection: Geophysical Journal of the Royal Astronomical Society, v. 59, p. 171–203. doi: 10.1111/j.1365-246X.1979.tb02560.x
Sleep, N.H., 1979, Thermal history and degassing of the Earth; some simple calculations; Journal of Geology, v. 87, p. 671–686.
Sřámek, O., McDonough, W. F., Kite, E. S., Lekić, V., Dye, S. T., and, Zhong, S., 2013, Geophysical and geochemical constraints on geoneutrino fluxes from Earth's mantle: Earth and Planetary Science Letters, v. 361, p. 356–366.
Solomatov V. S., 1995, Scaling of temperature- and stress-dependent viscosity convection: Physics of Fluids, v. 7, p. 266–274.

Solomatov, V.S., and Moresi, L.-N., 1997, Three regimes of mantle convection with non-Newtonian viscosity and stagnant lid convection on the terrestrial planets: Geophysical Research Letters, v. 24, p. 1907-1910.

Steinbach, V. and Yuen, D. A., 1994, Effects of depth-dependent properties on the thermal anomalies produced in flush instabilities from phase transitions: Physics of the Earth and Planetary Interiors, v. 86, p. 165–183.

Stein, C., Schmalzl, J., and Hansen, U., 2004, The effect of rheological parameters on plate behavior in a self-consistent model of mantle convection: Physics of the Earth and Planetary Interiors, v. 142, p. 225–255.

Tackley, P. J., 1996, On the ability of phase transitions and viscosity layering to induce long wavelength heterogeneity in the mantle: Geophysical Research Letters, v. 23, p. 1985–1988.

Tackley, P. J., 2000, Self-consistent generation of tectonic plates in time- dependent, three-dimensional mantle convection simulations: Geochemistry, Geophysics, Geosystems, v. 1, doi:10.1029/2000GC000043.

Tackley, P. J., Stevenson, D. J., Glatzmaier, G. A., and Schubert, G., 1993, Effects of an endothermic phase transition at 670 km depth in a spherical model of convection in the Earth's mantle: Nature, v. 361, p. 699–704.

Tan, E., Choi, E., Thoutireddy, P., Gurnis, M., Aivazis, M., 2006, GeoFramework: Coupling multiple models of mantle convection within a computational framework: Geochemistry Geophysics, Geosystems, v. 7.

Torrance, E. and Turcotte, D. L., 1971, Thermal convection with large viscosity variations: Journal of Fluid Mechanics, v. 47, p. 113-125.

Trompert, R., and Hansen, U., 1998, Mantle convection simulations with rheologies that generate plate-like behavior: Nature, v. 395 p. 686–689.

Turcotte, D. L., 1980, On the thermal evolution of the Earth: Earth and Planetary Science Letters, v. 48, p. 53–58.

Turcotte, D.L., and Oxburgh, E.R., 1967, Finite amplitude convection cells and continental drift: Journal of Fluid Mechanics, v. 28, p. 29â€“-42, doi: 10.1017/ S0022112067001880.

Turcotte, D.L., and Schubert, G., 2002, Geodynamics: Cambridge, Cambridge University Press.

van Heck, H., and Tackley, P. J., 2008, Planforms of self-consistently generated plate tectonics in 3-D spherical geometry: Geophysical Research Letters, v. 35, L19312. doi:10.1029/2008GL035190.

van Heck, H. and Tackley, P. J., 2011, Plate tectonics on super-Earths: Equally or more likely than on Earth. Earth and Planetary Science Letters, v. 310, p. 252-261.

van Hunen, J., van den Berg, A. P., and Vlaar, N. J., 2001, Latent heat effects of the major mantle phase transitions on low-angle subduction: Earth and Planetary Science Letters, v. 190, p. 125–135.

Wen, L. and Anderson, D. L., 1997, Layered mantle convection: A model for geoid and topography and seismology: Earth and Planetary Science Letters, v. 146, p. 367–377.

Wen, L. and Anderson, D. L., 1997, Present-day Plate Motion Constraint on Mantle Rheology and Convection: ,Journal of Geophysical Research, v. 102, p. 639–653.

Wessel, P. and Smith, W.H.F., 1998, New, improved version of the Generic Mapping Tools released: EOS Transactions of the AGU, v. 79, p. 579.

Zhang, N., Zhong, S., Leng, W. & Li, Z.-X., 2010, A model for the evolution of the Earth's mantle structure since the Early Paleozoic: Journal of Geophysical Research, v. 115, B06401.

Zhong, S.J., and Gurnis, M., 1994, The role of plates and temperature-dependent viscosity in phase change dynamics: Journal of Geophysical Research, v. 99, p. 15,903–15,917.

Zhong, S.J., and Gurnis, M., 1992, Viscous flow model of a subduction zone with a faulted lithosphere: long and short wavelength topography, gravity and geoid: Geophysical Research Letters, v. 19, 1891–1894.

Zhong, S., and Zuber, M. T., 2001, Degree-1 mantle convection and the crustal dichotomy on Mars: Earth and Planetary Science Letters, v. 189, p. 75–84.

Zhong, S., Zuber, M.T., Moresi, L., Gurnis, M., 2000, Role of temperature-dependent viscosity and surface plates in spherical shell models of mantle convection: Journal of Geophysical Research, v. 105, p. 11,063–11,082.

Zhong, S., McNamara, A., Tan, E., Moresi, L., Gurnis, M., 2008, A benchmark study on mantle convection in a 3-D spherical shell using CitcomS: Geochemistry Geophysics Geosystems v. 9.

Zhong, S., N. Zhang, Z.-X. Li, and Roberts, J. H., 2007, Supercontinent cycles, true polar wander, and very long-wavelength mantle convection: Earth and Planetary Science Letters, v. 261, p. 551–564.

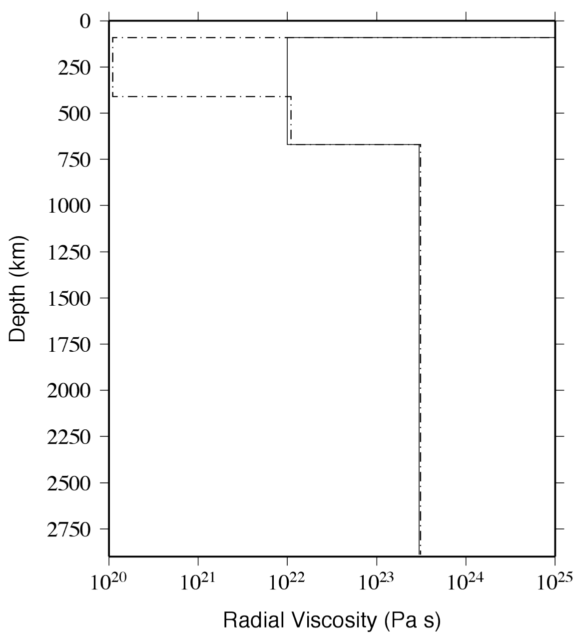

Figure 1: Radial viscosity plots used in the calculations. The black line is the stagnant-lid, no asthenosphere model, the red line is the model based on Höink and Lenardic (2008) producing a semi-mobile lid.

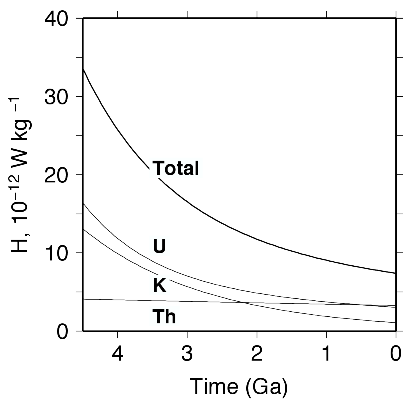

Figure 2: Radiogenic heat production (H) through time based on Turcotte and Schubert (2002). U denotes the contribution from uranium including both isotopes U^{235} and U^{238} Convection Plumes in the isotopes; Th denotes the contribution from thorium; and K denotes the contribution from potassium.

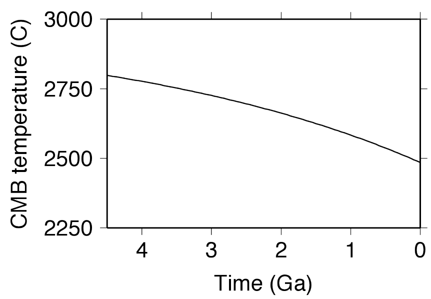

Figure 3: Core-mantle boundary temperature through time based on Davies (1980).

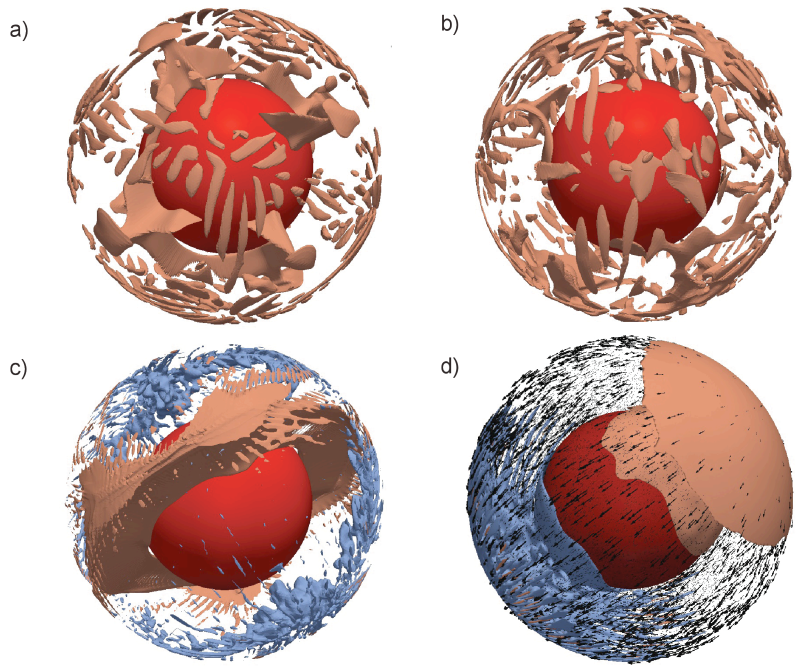

Figure 4: Isosurfaces of a temperature anomaly (relative to the mean temperature with depth) for models a) constant heating rate and core-mantle boundary temperature with no asthenosphere (solid black line in Figure 1) (DLA0), b) heating rate following Figure 2 and core-mantle boundary temperature following Figure 3 with no asthenosphere (solid black line in Figure 1) (DLA1), c) DLA2 is otherwise identical to DLA1 except for a low viscosity asthenosphere (dashed line in Figure 1) and d) otherwise identical to DLA2 except for a low viscosity in the lithosphere to enable mobile lid convection (DLA4) . The orange isotherm is 200 degrees above the mean temperature and the blue isotherm is 200 degrees below the mean temperature. These isotherms were taken after approximately 4 billion years of model evolution when the calculations had settled down into a stable pattern. In d) DLA4 I plot arrows showing the pattern of the near surface velocity.

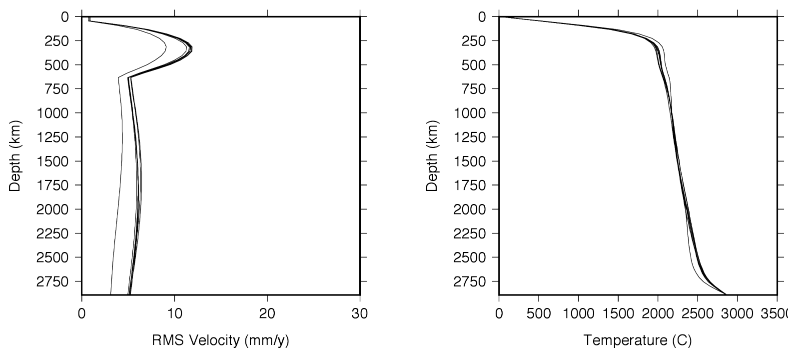

Figure 5: Horizontally averaged velocity (equation 6) (left) and temperature (equation 5) (right) profiles for calculation DLA0, constant heating rate and core-mantle boundary temperature with no asthenosphere (solid black line in Figure 1). Curves are shown for every 500 Myr of model evolution. A 0.3 K/km adiabatic gradient is added to the temperature to facilitate comparison with the geotherm.

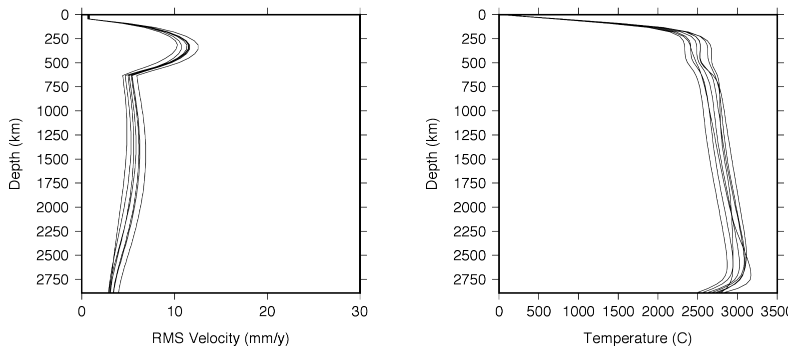

Figure 6: Horizontally averaged velocity (equation 6) (left) and temperature (equation 5) (right) profiles for calculation DLA1, heating rate following Figure 2 and core-mantle boundary temperature following Figure 3 with no asthenosphere (solid black line in Figure 1). Curves are shown for every 500 Myr of model evolution. A 0.3 K/km adiabatic gradient is added to the temperature to facilitate comparison with the geotherm.

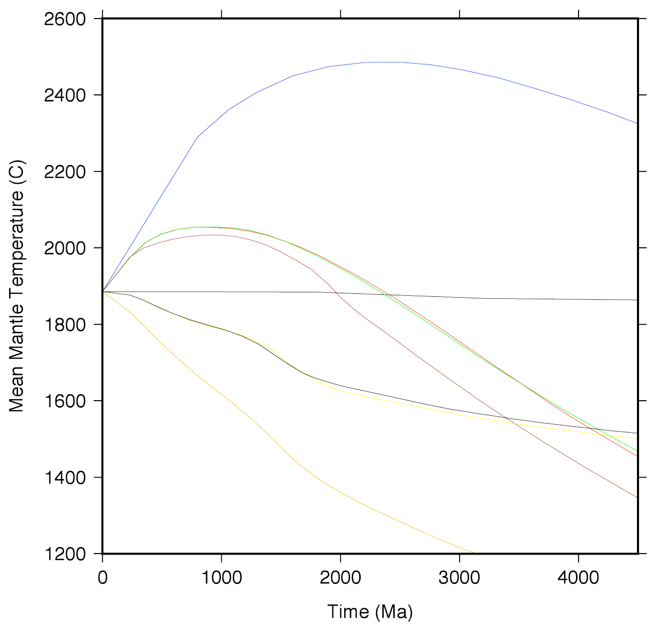

Figure 7: Mean temperature as a function of time for models DLA0 (black), DLA1 (blue), DLA2 (red), DLA3 (green), DLA4 (brown), DLA5 (orange), DLA6 (yellow), DLA7 (black).

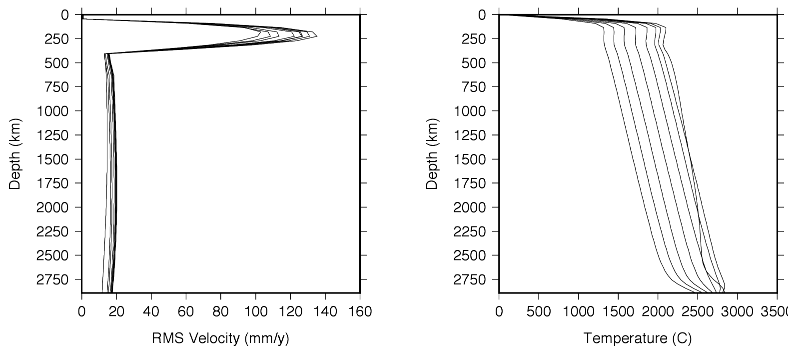

Figure 8: Horizontally averaged velocity (equation 6) (left) and temperature (equation 5) (right) profiles for calculation DLA2, heating rate following Figure 2 and core-mantle boundary temperature following Figure 3 with asthenosphere (dashed-dot line in Figure 1). Curves are shown for every 500 Myr of model evolution. A 0.3 K/km adiabatic gradient is added to the temperature to facilitate comparison with the geotherm.

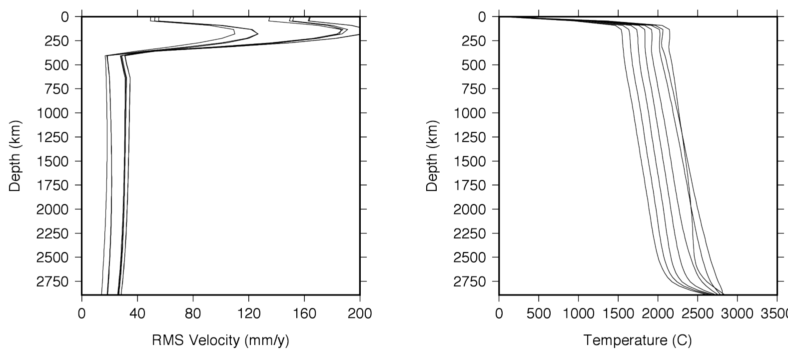

Figure 9: Horizontally averaged velocity (equation 6) (left) and temperature (equation 5) (right) profiles for calculation DLA4, heating rate following Figure 2 and core-mantle boundary temperature following Figure 3 with an asthenosphere (dashed-dot line in Figure 1) and a weak lithosphere. Curves are shown for every 500 Myr of model evolution. A 0.3 K/km adiabatic gradient is added to the temperature to facilitate comparison with the geotherm.

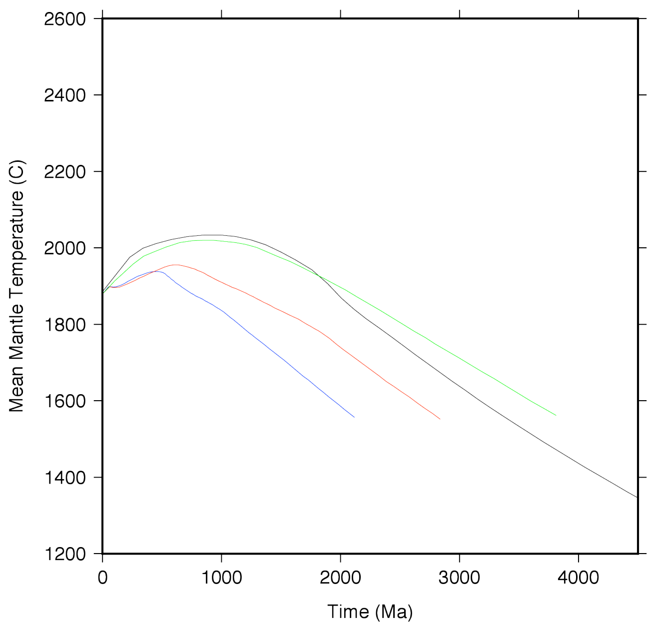

Figure 10: Mean temperature as a function of time for models DLA4 (black), DLA9 (blue), DLA10 (red), DLA11 (green).

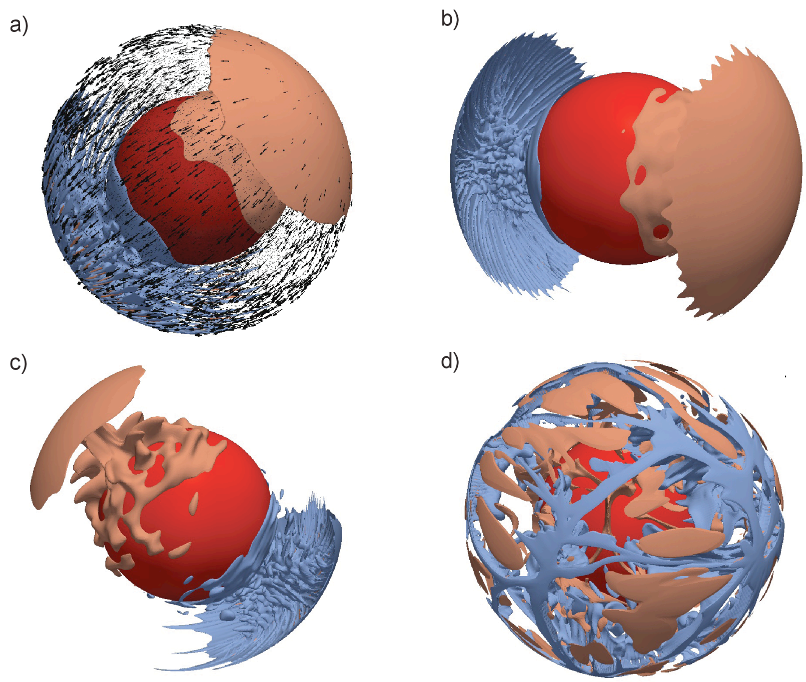

Figure 11: Isosurfaces of a temperature anomaly (relative to the mean temperature with depth) for calculations a) DLA4 heating rate following Figure 2 and core-mantle boundary temperature following Figure 3 with an asthenosphere (dashed-dot line in Figure 1) and weak lithosphere, b) DLA9, identical to DLA4 except an increase in Rayleigh number by a factor of 10, c) DLA10, identical to DLA9 except the asthenosphere viscosity is 0.03 times the reference viscosity, d) DLA11, identical to DLA10 except the asthenosphere viscosity is 0.3 times the reference viscosity. The orange isotherm is 200 degrees above the mean temperature and the blue isotherm is 200 degrees below the mean temperature. These isotherms were taken after approximately 4 billion years of model evolution when the calculations had settled down into a stable pattern. a) DLA4 is identical to Figure 4d and is repeated for comparison.

Model Parameters	Earth Value
reference density	3.8×10^3 kg/m^3
thermal expansion coef.	2.0×10^{-5} K^{-1}
surface gravity	10 m/s^2
surface temperature	273 K
convective temp drop	2000 K
depth of the mantle	2.890×10^6 m
thermal diffusivity	10^{-6} m^2/s
reference viscosity	10^{22} Pa s
Rayleigh number	3.5×10^7

Table 1: **Model Parameters**

Model	Lithosphere Viscosity η_l	Asthenosphere Viscosity η_a	CMB Temperature t_{cmb}	Heat Production H (10^{-12} W/kg)
DLA0	1000	1	const	8
DLA1	1000	1	decr.	radio
DLA2	1000	0.01	decr.	radio
DLA3	100	0.01	decr.	radio
DLA4	10	0.01	decr.	radio
DLA5	10	0.01	decr.	8
DLA6	10	0.01	decr.	16
DLA7	10	0.01	const	16
DLA9	10	0.01	decr.	radio
DLA10	10	0.03	decr.	radio
DLA11	10	0.3	decr.	radio

Table 2: Parameters for **D**ynamic **L**ithosphere **A**sthenosphere models. Lithosphere and asthenosphere viscosities are normalized to 10^{21} Pa s. CMB temperature is either constant, in which case a non-dimensional value of 2573 K is used, or decreases following Figure 2. The rate of heat production is either constant with time, in which case the value is given the table or 'radio'genic in which case the total curve (black line) from Figure 1 is used. For DLA9-11 the Rayleigh number is a factor of 10 higher than the value used in DLA0-7.